Iranian Journal of Analytical Chemistry
Volume 12, Issue 2, September 2026 (94-104) Original Research Article

مجله ایرانی شیمی تجزیه
دوره ۱۲، شماره ۲، مهر ۱۴۰۴ (۱۰۴-۹۴)

Green synthesized Copper Oxide Nanoparticles as Potential Nanocarriers for Anti-cancer Agent 5-Fluorouracil

Effat Esmaeili Shahri

Department of Chemistry, Payame Noor University, Tehran, Iran.

Received: 2 August 2025 **Accepted:** 13 September 2025
DOI: 10.30473/IJAC.2026.78642.1351

Abstract
Copper oxide nanoparticles were prepared by a green sol-gel method employing aqueous *Cressa cretica* leaf extract and copper(II) nitrate trihydrate as the copper precursor. The resulting nanoparticles were subsequently used as carriers for the anticancer drug 5-fluorouracil (5-FU). Physicochemical characterization was performed by Fourier-transform infrared spectroscopy (FTIR), ultraviolet–visible (UV–Vis) spectroscopy, X-ray diffraction (XRD), field-emission scanning electron microscopy coupled with energy-dispersive X-ray spectroscopy (FESEM/EDX), dynamic light scattering (DLS), zeta potential measurements, and thermogravimetric/differential thermal analysis (TGA/DTA). Drug-loading efficiency was quantified by high-performance liquid chromatography (HPLC), and the influence of reaction medium pH, contact time, and nanoparticle concentration on loading performance was systematically investigated to identify optimal conditions. The synthesized CuO nanoparticles were spherical, highly pure, and possessed a cubic crystalline structure, with a mean particle size of approximately 39 nm and a zeta potential of -15.6 mV. Under optimal loading conditions (pH 5.50, 5 h contact time, 0.015 g of CuO nanoparticles), approximately 40% of 5-FU was adsorbed onto the nanoparticle surface. MTT cytotoxicity assay demonstrated concentration-dependent cell death in Huh-7 hepatocellular carcinoma cells, with an IC_{50} of approximately 250 mg/L, a result consistent with an acceptable biocompatibility profile.

Keywords
Green method-Cressa cretica-CuO-NPs-Drug loading-5-fluorouracil.

1. Introduction

Cancer remains among the most therapeutically challenging diseases worldwide. Hundreds of millions of new cases are diagnosed annually, and more than half of those patients ultimately succumb to the disease [1]. Established treatment modalities include surgery, radiation therapy, chemotherapy, and bone marrow transplantation [2]. Despite the continued development of novel therapeutic strategies, chemotherapy remains the most widely employed approach to cancer management [3]. Its clinical utility, however, is substantially limited by the poor selectivity and systemic toxicity of most chemotherapeutic agents. Compounding these limitations, the capacity of cancer cells to acquire resistance to cytotoxic drugs further compromises treatment efficacy [4, 5].

5-Fluorouracil (5-FU) is a pyrimidine analogue that has long been used as a frontline chemotherapeutic agent. It exerts its antiproliferative effect by disrupting both DNA and RNA synthesis [6]. Nevertheless, the clinical effectiveness of 5-FU is constrained by its rapid metabolic degradation—reflected in a short biological half-life—and by its poor tumor selectivity [7].

These pharmacokinetic shortcomings necessitate the administration of elevated doses to achieve the desired therapeutic response, which in turn amplifies systemic toxicity [8].

Employing nano-carriers for tumor-targeted drug delivery has emerged as a powerful strategy to increase the bioavailability of chemotherapy agents [9, 10]. Nanoparticles are particularly well-suited to biological applications by virtue of their high surface-to-volume ratio, their capacity to interact with molecular and cellular processes, and their ability to modulate biological activity at the nanoscale [11]. Drug delivery science is a rapidly evolving discipline; despite substantial progress, however, the design of carriers that combine delivery efficiency with a favorable benefit-to-risk profile remains a significant formulation challenge [12]. Nanoscale drug delivery platforms offer a practical route to mitigating the adverse effects of chemotherapy while simultaneously improving therapeutic results [13]. Metallic nanoparticles are especially attractive for this purpose, as they confer enhanced drug solubility and bioavailability,

* Corresponding author:
E. Esmaeili Shahri; E-mail: ef.esmaili@yahoo.com

prolonged systemic circulation, site-selective biodistribution, and a reduced adverse-effect burden [14].

Green synthesis of metallic nanoparticles has attracted growing attention in bionanotechnology, offering economic and environmental advantages over traditional chemical and physical fabrication routes [15]. Recent research has explored eco-compatible methods for the preparation and surface modification of metal nanocarriers, encompassing silver [16], gold [17], platinum [18], copper [19], zinc oxides [20], and metal sulfide nanoparticles [21-23]. Biological resources employed in these approaches include diverse plant organs—roots, fruits, leaves, stems, and flowers—as well as microorganisms such as bacteria [24]. Green synthesis protocols are generally simple, rapid, and yield products of good stability. A central tenet of green chemistry is that particles produced by such routes exhibit improved biocompatibility and that the elimination of hazardous reagents prevents environmental contamination [25].

CuO nanoparticles are amenable to green-chemical synthesis in which plant extracts serve simultaneously as reducing, capping, and stabilizing agents. A variety of extracts have been employed to this end, including those from *Moringa oleifera*, *Averrhoa carambola*, *Psidium guajava and Catha edulis;* the efficacy of these materials is attributed to their content of bioactive phytochemicals—polyphenols, flavonoids, alkaloids, proteins, and terpenoids— which mediate the conversion of copper salts to CuO nanoparticles.

The present study aimed to develop a green, straightforward, and cost-effective synthesis of CuO nanoparticles using *Cressa cretica (C. cretica)* leaf extract and, to our knowledge, reports for the first time the application of this extract in CuO nanoparticles fabrication.

Cressa cretica is a small, halophytic plant of the family Convolvulaceae, distributed across arid, saline, and coastal habitats in regions including the Indian subcontinent, the Middle East, and North Africa. Its tolerance of harsh, salt-rich environments is well documented. Phytochemical investigations of C. cretica have identified a broad spectrum of bioactive and nutritional components, among them flavonoids, alkaloids, tannins, sterols, various sugars, proteins, and carbohydrates, as well as cardiac and anthraquinone glycosides, coumarin derivatives, and notably high concentrations of mineral salts. This rich phytochemical profile equips the extract to function concurrently as a reducing agent, a complexing agent, and a stabilizing (capping) agent. Although green synthesis of copper oxide nanoparticles, various plant extracts are well established, reports describing the specific use of C. cretica extract as a capping agent in this context remain scarce in literature.

The primary objective of this work was to load the drug 5-FU onto CuO nanoparticles biosynthesized with aqueous C. cretica extract to exploit nanoparticles as drug nanocarriers. This approach is expected to enhance therapeutic efficacy, permit the use of reduced drug doses, and minimize the adverse effects associated with systemic 5-FU administration. The nanoparticles were characterized by multiple spectroscopic and analytical techniques, and their biocompatibility was evaluated in Huh-7 hepatocellular carcinoma cells.

2. Experimental

2.1. Chemicals and Apparatus

5-Fluorouracil (5-FU), copper(II) nitrate trihydrate ($Cu(NO_3)_2$ $3H_2O$), trypsin, and phosphate-buffered saline (PBS) were purchased from Sigma-Aldrich and utilized as received without further purification.

Both CuO nanoparticles and 5-FU@CuO nanoparticles were characterized using the following techniques. Surface functional groups were identified by Fourier-transform infrared spectroscopy (FT-IR 8400, Shimadzu, Japan). Crystalline structure was determined by an X'pert diffractometer (Philips). Zeta potential measurements were carried out on a Malvern Nano ZS-90 instrument (Malvern Instruments, UK). Morphological features characterization was performed by Field Emission Scanning Electron Microscopy (FESEM; Hitachi S4160, Japan), with elemental composition and mapping obtained simultaneously by Energy Dispersive X-ray Spectrometer (EDX) using the detector attached to the FESEM system. Thermogravimetric and differential thermal analysis (TGA/DTA) were conducted on MIRAIII, SAMX, and TESCAN instruments. The concentration of 5-FU loaded onto CuO nanoparticles, and the optimization of drug-loading parameters were determined by high-performance liquid chromatography (HPLC) on an Agilent Infinity 1260 system equipped with a Waters XTerra RP18 column (250 × 4.6 mm, 5 μm) and a photodiode-array detector operating at a UV detection wavelength of 266 nm. The mobile phase consisted of 50 mM potassium phosphate buffer (pH 3.3), delivered isocratically at a flow rate of 1.0 mL/min.

2.2 Preparation of CuO Nanoparticles

Leaves of C. cretica were collected from Sabzevar District, Khorasan Razavi Province, Iran. To prepare the plant extract, the leaves were first washed repeatedly with distilled water to remove surface contaminants and then dried in the shade

DOI: 10.30473/IJAC.2026.78642.1351

for 10 days. The air-dried leaves were ground to a fine powder, and extraction was carried out by percolation using distilled water as the solvent at a plant-to-solvent ratio of 1:10 (w/v). Specifically, 10 g of powdered leaves were dispersed in 100 mL of distilled water and stirred for 6 h. The resulting aqueous extract was filtered through Whatman filter paper and stored at 4 °C until further use. The soluble solid content of the extract, measured as Degree Brix, was 2.31%.

For nanoparticle synthesis, 20 mL of *C.* cretica extract solution was added dropwise to 80 mL of an aqueous 0.5 M $Cu(NO_3)_2.3H_2O$ solution, upon which the color of the copper salt solution shifted from blue to blue-green. The mixture was subsequently stirred in an oil bath at 72 ˚C for 5 h to form a gel, which was then dried at 50 ˚C for 4 h. The resulting precipitate was finally calcined in a furnace at 500 °C for 2 h (Fig. 1).

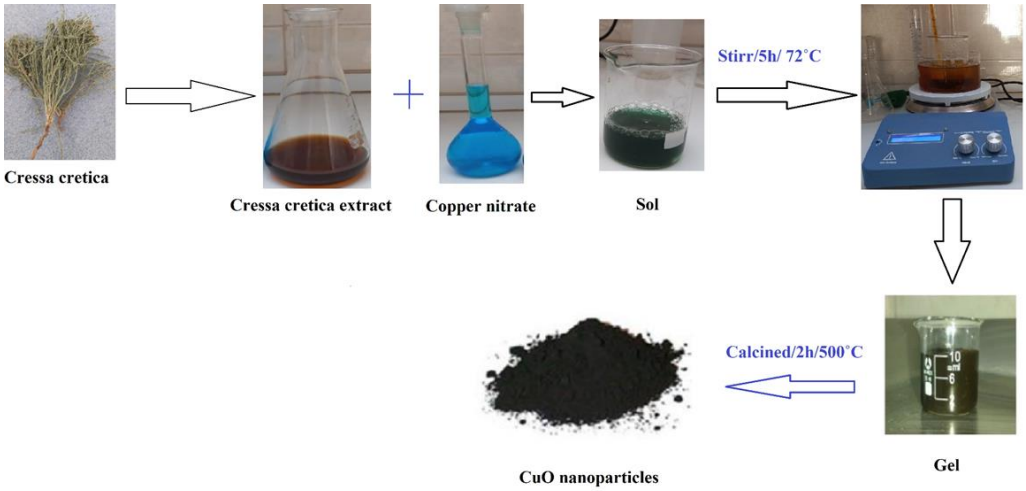

Fig. 1. Schematic of the synthesis of CuO nanoparticles

2.3. Preparation of 5-FU-Loaded CuO Nanoparticles and Calibration Curve

A stock solution of 5-FU (1000 µg/mL) was prepared by dissolving 0.025 g of the drug in 25 mL of ethanol. This stock was then diluted with 50 mM KH_2PO_4 buffer to produce working standard solutions spanning the concentration range of 100–700 µg/mL. Each solution was injected into the HPLC system, and the corresponding chromatograms were recorded. Peak areas were measured, and a calibration curve was constructed by plotting peak area against drug concentrations (Fig. 2) [26].

For drug-loading experiments, varying amounts of CuO nanoparticles (0.002–0.04 g) were added to the drug solutions and stirred for contact times ranging from 0.5 to 24 h. The suspensions were then centrifuged for a sufficient time, and the supernatant from each was carefully separated. The residual free drug concentration in the supernatant was quantified against the 5-FU calibration curve, and the entrapped drug amount was calculated as the difference between the total and free drug quantities. Drug loading efficiency (DL%) was calculated according to Equation 1 [1]:

$$DL\% = \frac{\text{Total drug amount} - \text{Free drug amount}}{\text{Weight of NPs}} \times 100 \quad (1)$$

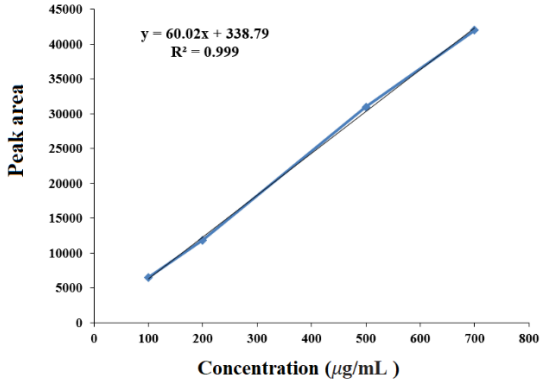

Fig. 2. Calibration curve of 5-FU

2.4. Optimization of 5-FU Loading onto CuO Nanoparticles

2.4.1. Effect of Reaction Medium pH

Solution pH is known to exert a significant influence on drug adsorption behavior [27]. Accordingly, drug loading was evaluated across a pH range of 3–10. In each experiment, 0.01 g of CuO nanoparticles was added to 5 mL of 5-FU solution (0.01 M), and the pH was adjusted to the target value using either 0.1 M HCl or 0.1 M NaOH. The suspensions were stirred at 300 rpm for 5 h, after which the drug loading percentage was determined as described above. Based on these results, pH 5.50 was identified as the optimal condition and adopted for subsequent experiments.

DOI: 10.30473/IJAC.2026.78642.1351

2.4.2. Effect of Drug Loading Time

CuO nanoparticles (0.01 g) were dispersed in 5 mL of 5-FU solution (0.01 M) at pH 5.50, adjusted with 0.1 M HCl, and the suspension was stirred at 300 rpm for contact times ranging from 1 to 20 h. After calculating the drug loading percentage at each time point, a loading time of 5 h was selected as optimal for subsequent experiments.

2.4.3. Effect of Nanoparticle Amount

To determine the optimal nanoparticle loading, experiments were conducted with CuO nanoparticle masses of 0.005, 0.01, 0.015, and 0.02 g, each added to 5 mL of 5-FU solution. The pH of each suspension was adjusted to 5.50, and the mixture was agitated for 5 h. An optimal nanoparticle mass of 0.015 g was identified from these experiments.

2.5. Cytotoxicity Assay

The MTT assay assessed the cytotoxic effect of CuO nanoparticles on Huh-7 hepatocellular carcinoma cells. Cells were seeded in 96-well plates at a density of 2×10^4 cells per well in the appropriate volume of culture medium and incubated at 37 °C in a humidified 5% CO_2 atmosphere for 48 h. Cells were then exposed to CuO nanoparticles at concentrations ranging from 0 to 1000 mg/L; control wells received PBS. Following a 4 h incubation at 37 °C, MTT reagent was added to each well, and the plates were incubated in the dark for a further 4 h. Formazan crystals were subsequently dissolved by adding 40 µL of DMSO to each well. Absorbance was measured at 570 nm using an ELISA plate reader. The half-maximal inhibitory concentration (IC_{50}) was defined as the nanoparticle concentration that produced a 50% reduction in cell viability relative to the untreated control (zero concentration). Results are expressed as percentage cell viability as a function of nanoparticle concentration (mg/L) [28].

3. Results and Discussion

3.1. Characterization of the Prepared Nanoparticles

In this section, the structural properties of the prepared nanoparticles, which are central to understanding both their synthesis and functional performance, were evaluated by FT-IR spectroscopy, UV–Vis spectroscopy, XRD, FESEM/EDX, DLS, zeta potential measurements, and TGA/DTA analysis. The optimal conditions for 5-FU loading were subsequently investigated.

3.1.1. FT-IR Analysis

FT-IR spectroscopy was employed to identify the characteristic functional groups of 5-FU and CuO nanoparticles and to probe the interactions arising upon drug loading. The FT-IR spectrum of 5-FU (Figure 3) exhibited absorption bands at 3139 and 2937 cm^{-1} attributable to symmetric N-H and asymmetric C-H stretching vibrations, respectively [29]. Stretching vibrations associated with C=O, C-N, and C-F bonds were observed at 1658, 1426, and 1241 cm^{-1}, respectively [30].

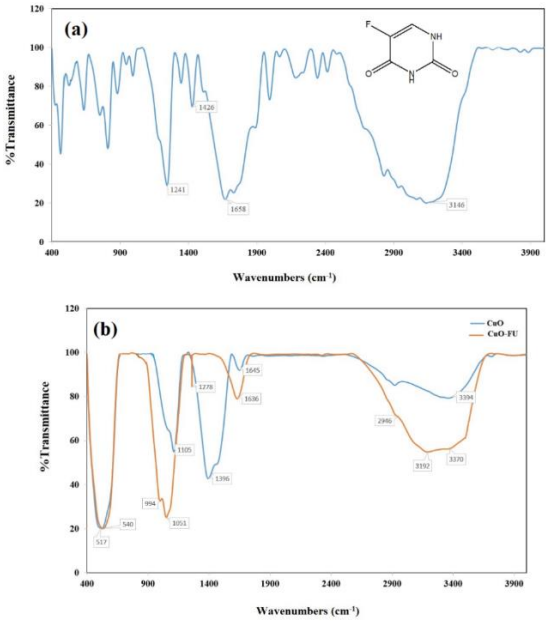

Figure 3. The FT-IR spectra of (a) 5-FU and (b) CuO nanoparticles and CuO-FU

The FT-IR spectrum of CuO nanoparticles (Figure 2a) displayed a broad absorption at 3437 cm^{-1} arising from hydroxyl (O–H) stretching, while bands at 1640 cm^{-1} and 1398 cm^{-1} are assigned to the bending vibration of adsorbed water molecules, indicating surface moisture uptake [31]. The characteristic Cu-O stretching vibration of CuO appeared at 517 cm^{-1} [32]. In the spectrum of the 5-FU@CuO composite (Figure 2b), bands attributable to both components are present, with 5-FU-related absorptions observed at 3192, 2946, 1636, and 1278 cm^{-1}, corresponding to symmetric N-H stretching, asymmetric C-H, C=O stretching, and C-F stretching vibrations, respectively. Notably, the N–H and C=O stretching bands shifted by 53 cm^{-1} to higher and 22cm^{-1} to lower wavenumbers, respectively, upon drug loading onto the nanoparticle surface. This shift is indicative of involvement of the amide group in coordination with the metal center [33].

The adsorption of 5-FU onto the CuO nanoparticles is likely governed by multiple intermolecular interactions. The carbonyl oxygen and nitrogen atoms of 5-FU can coordinate with surface Cu^{2+} ions, while the N–H and C=O groups participate in hydrogen bonding with surface hydroxyl groups. In addition, electrostatic interactions at the optimized loading pH (5.5) may further stabilize the adsorbed drug molecules. The

DOI: 10.30473/IJAC.2026.78642.1351

observed shifts in the FT-IR absorption bands together with the change in zeta potential after drug loading provide indirect evidence supporting these interactions.

3.1.2 XRD Analysis

The crystalline structure of the prepared CuO nanoparticles was examined by XRD. The diffraction pattern (Figure 4) displayed eleven distinct peaks at 2θ values of 32.48°, 35.51°, 38.68°, 48.82°, 53.43°, 58.24°, 61.55°, 65.68°, 66.28°, 68.01°, and 75.12°, all of which are in good agreement with the characteristic reflections of the cubic phase of CuO according to JCPDS card no. 01-072-0629 [34]. The sharpness and intensity of the diffraction peaks confirm the crystalline nature of the synthesized nanoparticles. Applying the Debye-Scherer equation ($D = K\lambda/\beta\cos\theta$) [35], the estimated crystalline size was estimated to be approximately 29.12 nm.

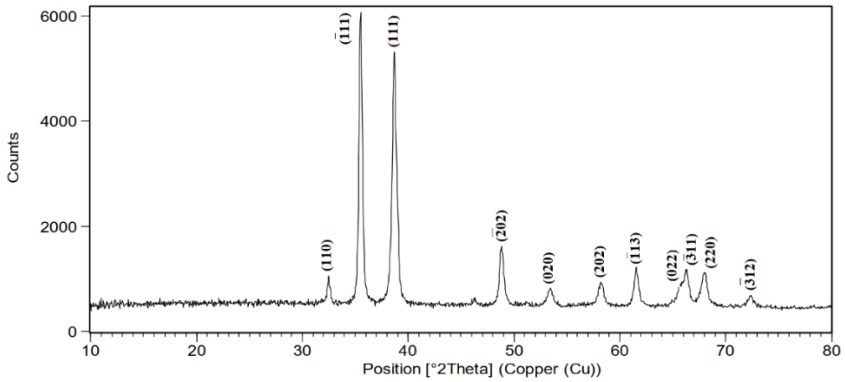

Figure 4. The XRD patterns of CuO nanoparticles

3.1.3. FESEM and EDX Analysis

The morphology of CuO nanoparticles was assessed by FESEM. The particles exhibited a nearly spherical morphology with a uniform size distribution and a smooth surface texture (Figure 5a). Particle size distribution analysis from the corresponding histogram yielded a mean particle size of 39 nm (Figure 5b).

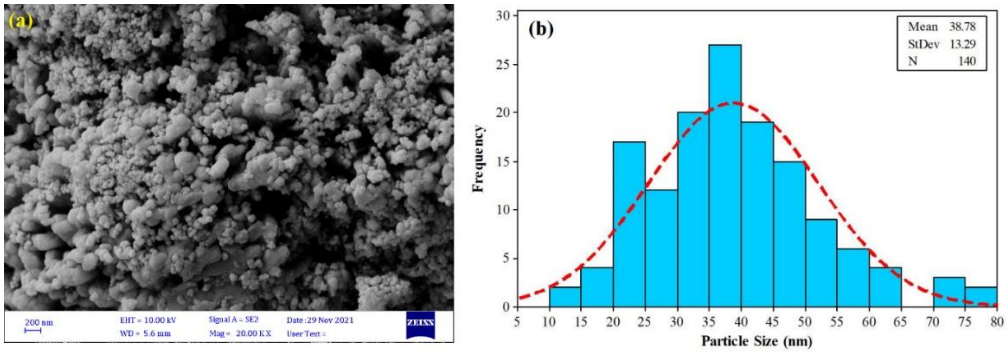

Figure 5. (a) FESEM image and (b) the particle size distribution diagram of CuO nanoparticles

The EDX spectrum (Figure 6) showed only signals attributable to copper and oxygen, confirming the elemental purity of the product. A gold-related signal present in the spectrum originates from the thin gold coating applied to the sample surface prior to analysis, and the weak peak near 0.2 keV is attributed to trace carbon residues derived from the plant extract [19, 23].

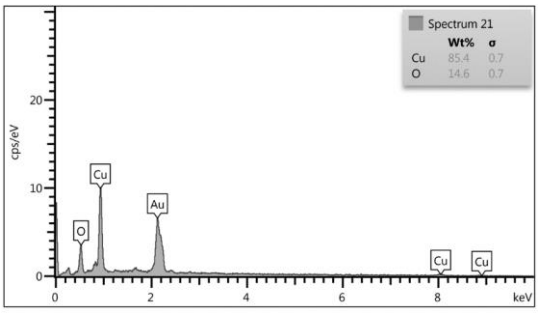

Figure 6. EDS analysis of CuO nanoparticles

3.1.4. UV-Vis Analysis

The optical absorption properties of the CuO nanoparticles were investigated over the

wavelength range of 250-650 nm. A characteristic absorption maximum was recorded at 276 nm in the UV region, consistent with the surface plasmon resonance (SPR) of CuO nanoparticles and in agreement with values reported in the literature [36, 37].

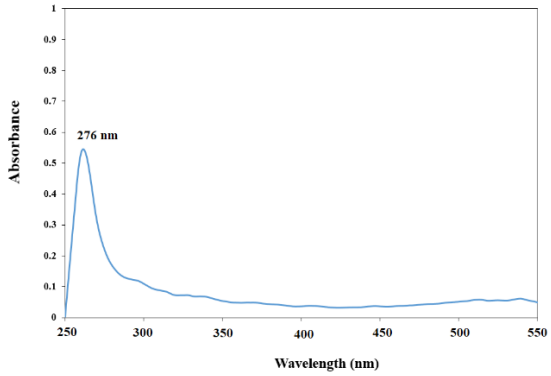

Figure 7. The UV-Vis spectra of CuO nanoparticles

3.1.5. DLS and Zeta Potential Analysis

The hydrodynamic diameter and surface charge of the nanoparticles were determined by DLS and zeta potential measurements, respectively. CuO nanoparticles and 5-FU@CuO exhibited mean hydrodynamic diameters of approximately 119 nm and 184 nm, respectively (Table 1 and Figure 8). The polydispersity index (PDI) fell within the range of 0.2-0.4 for both samples, indicative of a reasonably uniform particle size distribution in suspension [38]. At neutral pH, CuO nanoparticles carried a negative surface charge of -15.6 mV, whereas 5-FU@CuO displayed a positive zeta potential of +16.1 mV (Table 1 and Figure 9).

The negative zeta potential of the unloaded nanoparticles reflects their intrinsic surface electronegativity and contributes to colloidal stability by suppressing particle aggregation. The reversal to a positive zeta potential upon drug loading provides direct evidence for 5-FU adsorption onto the nanoparticle surface. This sign inversion is attributed to the interaction between the CuO surface and the amide group of the 5-FU molecule, forming an intermolecular complex that alters the surface charge distribution. The resulting positive surface charge promotes improved colloidal dispersibility, enhanced cellular uptake, and more selective drug delivery, collectively contributing to improved safety and therapeutic performance [39].

Table 1. DLS and zeta potential data of CuO-NPs and CuO-FU

Name	Average size (nm)	Zeta potential (mV)	PDI
CuO	119	-15.6	0.220
CuO-FU	184	+16.1	0.350

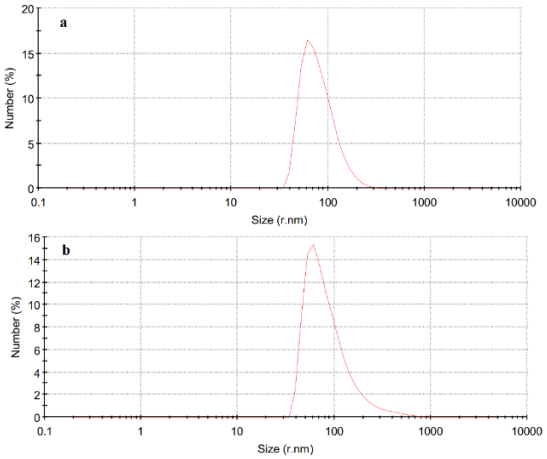

Figure 8. DLS analysis of (a) CuO-NPs and (b) CuO-FU

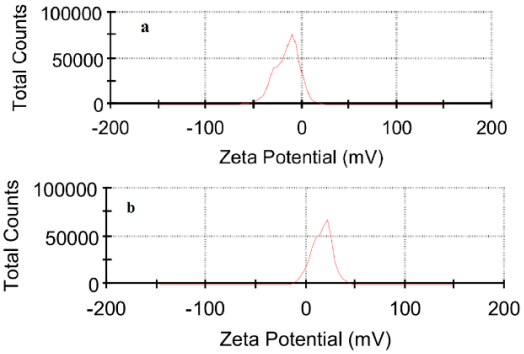

Figure 9. Zeta potential of (a) CuO-NPs and (b) CuO-FU

3.1.6. TGA/DTA Analysis

The thermal behavior of the synthesized gel was analyzed by TGA/DTA over the temperature range of 25–800 °C (Figure 10). Weight loss proceeded through three distinct endothermic stages. The material was thermally stable up to 109 °C, beyond which decomposition commenced. In the first stage (109–182 °C), a weight loss of approximately 22% is attributed to the removal of adsorbed water molecules via an endothermic process. Decomposition of residual organic matter occurred in two subsequent endothermic stages: a loss of approximately 14% of the initial mass between 182 and 254 °C, followed by a further loss of approximately 11% between 254 and 380 °C, reflecting the progressive combustion of organic constituents and the formation of pure CuO phase. No further weight loss was observed between 500 and 800 °C, confirming that thermally stable CuO crystals constitute the final product [40, 41].

DOI: 10.30473/IJAC.2026.78642.1351

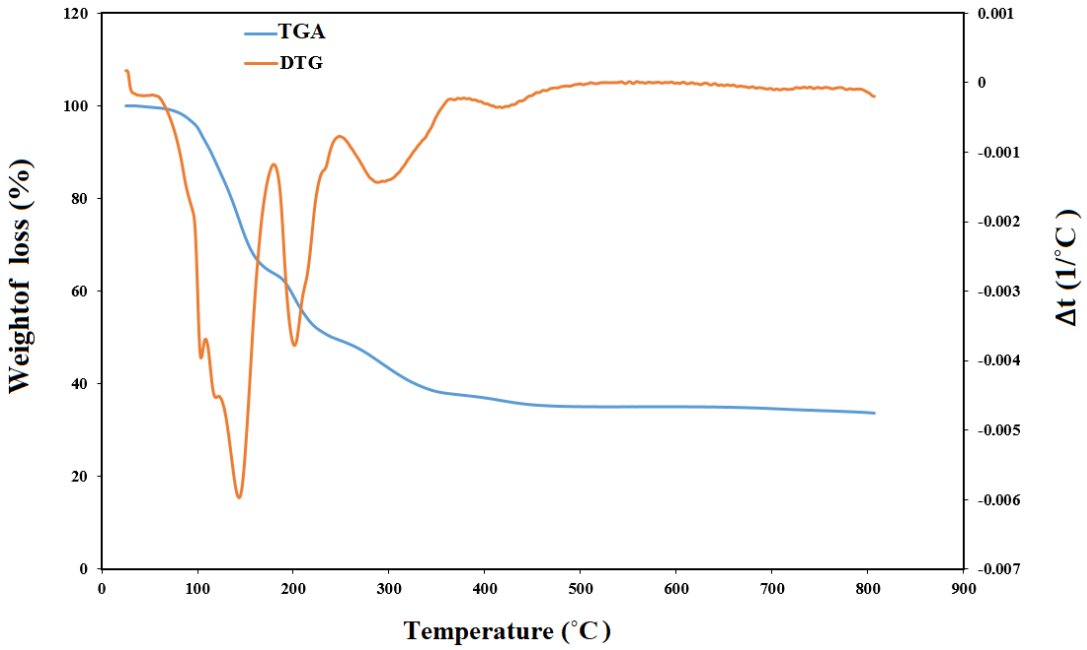

Figure 10. The TGA/DTA curves of the primary gel to obtain CuO-NPs

3.2. Drug Loading Efficiency Studies

The influence of three key parameters—pH, contact time, and nanoparticle mass—on the efficiency of 5-FU loading onto CuO nanoparticles was systematically investigated and optimized. Drug loading efficiency was first evaluated across a pH range of 3–10. As shown in Figure 11a, maximum drug loading was achieved at pH 5 and 6, with efficiency declining at higher pH values; accordingly, pH 5.50 was selected as the optimal value. Under strongly acidic conditions (pH 2–6), protonation of the CuO surface promotes partial dissolution, releasing 4.3–8.5% of Cu^{2+} ions into solution. Above pH 6, the solubility of CuO diminishes markedly, and the concentration of released copper ions decreases. This behavior reflects the inverse relationship between suspension pH and CuO solubility: at alkaline pH, the elevated hydroxyl ion concentration favors the formation of insoluble copper hydroxide complexes, which reduces the availability of active surface sites for drug adsorption [42].

The effect of contact time on drug loading was examined at reaction times of 1, 5, and 10 h. The highest drug loading efficiency, 38.60%, was attained at 5 h, reflecting the progressive increase in drug–nanoparticle interactions over time (Figure 11 b). Beyond 5 h, drug adsorption declined, an observation attributed to inter-particle aggregation at extended contact times, which reduces the accessible surface area [43].

Finally, the optimal nanoparticle mass was determined by testing amounts of 0.005, 0.01, 0.015, and 0.02 g of CuO nanoparticles. As illustrated in Figure 11c, drug loading efficiency increased with nanoparticle mass from 0.005 to 0.015 g, consistent with the greater total surface area available for drug adsorption. At 0.02 g, however, efficiency declined, likely due to nanoparticle aggregation driven by elevated surface energy at higher particle concentrations, which reduces the effective surface area [44]. Under the identified optimal conditions—pH 5.50, 0.015 g of CuO nanoparticles, and a contact time of 5 h —a drug loading efficiency of 40% was achieved.

DOI: 10.30473/IJAC.2026.78642.1351

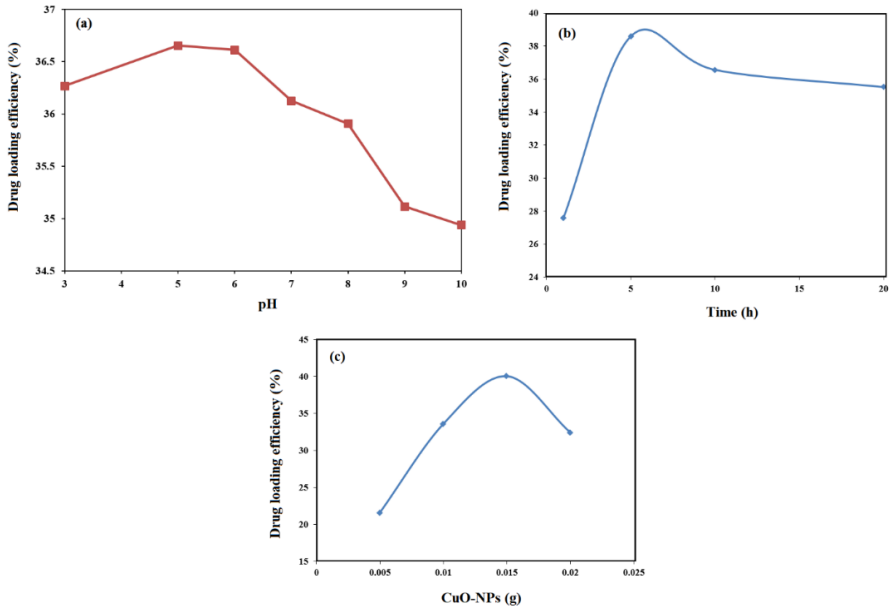

Figure 11. The drug loading percentages in three different conditions (a) pH, (b) the reaction time, and (c) the amounts of CuO nanoparticles

3.3. Cytotoxicity Evaluation

The cytotoxic activity of green-synthesized CuO nanoparticles against the Huh-7 hepatocellular carcinoma cell line was assessed by the MTT assay following 48 h of treatment (Figure 12). Cell viability decreased in a concentration-dependent manner across the tested dose range. The IC_{50} value for CuO nanoparticles in Huh-7 cells was approximately 250 mg/L, demonstrating potent anticancer activity against human liver cancer cells [45]. Although the present results demonstrate the cytotoxic effect of the green-synthesized CuO nanoparticles against Huh-7 cells, the biological evaluation was limited to the unloaded nanoparticles. Comparative cytotoxicity studies involving free 5-fluorouracil and 5-FU-loaded CuO nanoparticles were beyond the scope of the present work. Such investigations are important for determining whether nanoparticle-mediated drug loading enhances the therapeutic efficacy of 5-fluorouracil and will be the subject of future studies.

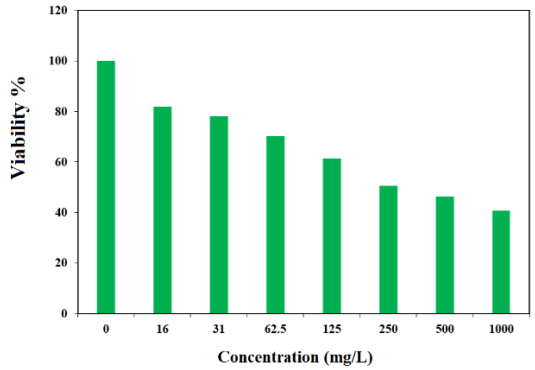

Figure 12. Cytotoxicity effect of CuO-NPs on Huh-7 cancer cell line via the MTT assay

4. Conclusions

CuO nanoparticles were prepared by a green sol-gel method using *Cressa cretica* extract and investigated as potential nanocarriers for 5-fluorouracil. The prepared CuO nanoparticles were identified using various spectroscopic methods, and their properties were determined. Comprehensive spectroscopic and physicochemical characterization established that the nanoparticles are phase-pure, possess a cubic crystalline structure, have a mean particle size of approximately 39 nm, and carry a surface charge of -15.6 mV. Drug loading onto the CuO surface was confirmed by FT-IR spectroscopy and zeta potential measurements. HPLC-based optimization identified pH 5.50, a nanoparticle mass of 0.015 g, and a contact time of 5 h as the optimal loading conditions, under which approximately 40% of 5-FU was adsorbed onto the nanoparticle surface. MTT cytotoxicity assays in Huh-7 cells demonstrated concentration-dependent cell death with an IC_{50} of approximately 250 mg/L, confirming the anticancer potential of the prepared CuO nanoparticles.

Despite the promising results obtained in this study, several aspects require further investigation to comprehensively evaluate the potential of the developed nanocarrier system. In particular, in vitro drug release studies under physiological and tumor-mimicking conditions will be performed in future work to investigate the release kinetics and delivery behavior of 5-fluorouracil from the CuO nanoparticles. Furthermore, comparative cytotoxicity studies involving free 5-fluorouracil, 5-FU-loaded CuO nanoparticles, and normal (non-cancerous) cell lines will be conducted to assess therapeutic efficacy, biocompatibility, and selectivity. These investigations will provide a more comprehensive understanding of the suitability of the developed green-synthesized

DOI: 10.30473/IJAC.2026.78642.1351

CuO nanoparticles as a potential drug delivery platform.

Acknowledgment
The author considers it necessary to thank and appreciate the abundant support of Payam Noor University of Iran.

CONFLICT OF INTEREST
"The authors declare that there are no conflicts of interest regarding the publication of this manuscript".

References
[1] S. Khaledi, S. Jafari, S. Hamidi, O. Molavi, S. Davaran, Preparation and characterization of PLGA-PEG-PLGA polymeric nanoparticles for co-delivery of 5-Fluorouracil and Chrysin, J Biomater. Sci., Polym. Ed. 31(9) (2020) 1107-1126.

[2] C. Jiang, K.R. Yabroff, L. Deng, Q. Wang, S. Perimbeti, C.L. Shapiro, X. Han, Self-reported Transportation Barriers to Health Care Among US Cancer Survivors, JAMA oncol. 8(5) (2022) 775-778.

[3] M. Arruebo, N. Vilaboa, B. Sáez-Gutierrez, J. Lambea, A. Tres, M. Valladares, A. González-Fernández, Assessment of the evolution of cancer treatment therapies, Cancers (Basel) 3(3) (2011) 3279-3330.

[4] J. Zugazagoitia, C. Guedes, S. Ponce, I. Ferrer, S. Molina-Pinelo, L. Paz-Ares, Current challenges in cancer treatment, Clin. ther. 38(7) (2016) 1551-1566.

[5] L.T.H. Phi, I.N. Sari, Y.-G. Yang, S.-H. Lee, N. Jun, K.S. Kim, Y.K. Lee, H.Y. Kwon, Cancer stem cells (CSCs) in drug resistance and their therapeutic implications in cancer treatment, Stem Cells Int. 2018 (2018).

[6] N. Thalambedu, Y. Khan, Fluorouracil (5-FU)-induced cardiomyopathy, Cureus 11(7) (2019).

[7] S.F. Rapa, G. Magliocca, G. Pepe, G. Amodio, G. Autore, P. Campiglia, S. Marzocco, Protective effect of pomegranate on oxidative stress and inflammatory response induced by 5-fluorouracil in human keratinocytes, Antioxid. 10(2) (2021) 203.

[8] K. Joshi, A. Chandra, K. Jain, S. Talegaonkar, Nanocrystalization: an emerging technology to enhance the bioavailability of poorly soluble drugs, Pharm. Nanotechnol. 7(4) (2019) 259-278.

[9] P. Dong, K. Rakesh, H. Manukumar, Y.H.E. Mohammed, C. Karthik, S. Sumathi, P. Mallu, H.-L. Qin, Innovative nano-carriers in anticancer drug delivery-a comprehensive review, Bioorg. Chem. 85 (2019) 325-336.

[10] E. Rostami, Progresses in targeted drug delivery systems using chitosan nanoparticles in cancer therapy: A mini-review, J. Drug Deliv. Sci. Technol. 58 (2020) 101813.

[11] D. Nath, P. Banerjee, Green nanotechnology–a new hope for medical biology, Environ. Toxicol. Pharmacol. 36(3) (2013) 997-1014.

[12] B. Felice, M.P. Prabhakaran, A.P. Rodriguez, S. Ramakrishna, Drug delivery vehicles on a nano-engineering perspective, Mater. Sci. Eng. C 41 (2014) 178-195.

[13] I. Khan, K. Saeed, I. Khan, Nanoparticles: Properties, applications and toxicities, Arab. J. Chem. 12(7) (2019) 908-931.

[14] V. Chandrakala, V. Aruna, G. Angajala, Review on metal nanoparticles as nanocarriers: current challenges and perspectives in drug delivery systems, Emergent Mater. (2022) 1-23.

[15] N. Shreyash, S. Bajpai, M.A. Khan, Y. Vijay, S.K. Tiwary, M. Sonker, Green Synthesis of Nanoparticles and Their Biomedical Applications: A Review, ACS Appl. Nano Mater. 4(11) (2021) 11428-11457.

[16] P.K. Palai, A. Mondal, C.K. Chakraborti, I. Banerjee, K. Pal, Green synthesized amino-PEGylated silver decorated graphene nanoplatform as a tumor-targeted controlled drug delivery system, SN Appl. Sci. 1(3) (2019) 1-18.

[17] S. Patra, S. Mukherjee, A.K. Barui, A. Ganguly, B. Sreedhar, C.R. Patra, Green synthesis, characterization of gold and silver nanoparticles and their potential application for cancer therapeutics, Mater. Sci. Eng. C 53 (2015) 298-309.

[18] T.C. Johnstone, K. Suntharalingam, S.J. Lippard, The next generation of platinum drugs: targeted Pt (II) agents, nanoparticle delivery, and Pt (IV) prodrugs, Chem. Rev. 116(5) (2016) 3436-3486.

[19] U. Goswami, A. Dutta, A. Raza, R. Kandimalla, S. Kalita, S.S. Ghosh, A. Chattopadhyay, Transferrin–copper nanocluster–doxorubicin nanoparticles as targeted theranostic cancer Nanodrug, ACS Appl. Mater. Interfaces. 10(4) (2018) 3282-3294.

[20] J. Hussein, M.F. Attia, M. El Bana, S.M. El-Daly, N. Mohamed, Z. El-Khayat, M.E. El-Naggar, Solid state synthesis of docosahexaenoic acid-loaded zinc oxide nanoparticles as a potential antidiabetic agent in rats, Int. J. Biol. Macromol. 140 (2019) 1305-1314.

[21] Q. Li, L. Sun, M. Hou, Q. Chen, R. Yang, L. Zhang, Z. Xu, Y. Kang, P. Xue, Phase-change material packaged within hollow copper sulfide nanoparticles carrying doxorubicin and chlorin e6 for fluorescence-guided trimodal therapy of cancer, ACS Appl. Mater. Interfaces. 11(1) (2018) 417-429.

[22] L. Hou, X. Shan, L. Hao, Q. Feng, Z. Zhang, Copper sulfide nanoparticle-based localized drug delivery system as an effective cancer synergistic treatment and theranostic platform, Acta Biomater. 54 (2017) 307-320.

[23] Z. Xie, D. Wang, T. Fan, C. Xing, Z. Li, W. Tao, L. Liu, S. Bao, D. Fan, H. Zhang, Black phosphorus analogue tin sulfide nanosheets: synthesis and application as near-infrared photothermal agents and drug delivery platforms for cancer therapy, J. Mater. Chem. B 6(29) (2018) 4747-4755.

[24] P. Mohanpuria, N.K. Rana, S.K. Yadav, Biosynthesis of nanoparticles: technological concepts and future applications, J NANOPART. RES. 10(3) (2008) 507-517.

[25] H. Duan, D. Wang, Y. Li, Green chemistry for nanoparticle synthesis, Chem. Soc. Rev. 44(16) (2015) 5778-5792.

[26] G. Singh, R.S. Pai, Optimization (central composite design) and validation of HPLC method for investigation of emtricitabine loaded poly (lactic-co-glycolic acid) nanoparticles: in vitro drug release and in vivo pharmacokinetic studies, Sci. World 2014 (2014).

[27] W. Hong, D. Chen, L. Jia, J. Gu, H. Hu, X. Zhao, M. Qiao, Thermo-and pH-responsive copolymers based on PLGA-PEG-PLGA and poly (L-histidine): synthesis and in vitro characterization of copolymer micelles, Acta Biomater. 10(3) (2014) 1259-1271.

[28] J.V. Meerloo, G.J. Kaspers, J. Cloos, Cell sensitivity assays: the MTT assay, Cancer cell culture, Springer 2011, pp. 237-245.

[29] M. Hakimi, M. Alikhani, M. Mashreghi, N. Feizi, H. Raeisi, Y. Mirzai, V. Eigner, M. Dusek, A heterodinuclear complex of sd block containing sodium(I), manganese(II) and the enrofloxacinate anion: Preparation, crystal structure and antibacterial activity, J. Mol. Struct. 1186 (2019) 355-361.

[30] B.-B. Wu, Y.-P. Gong, X.-H. Wu, Y.-Y. Chen, F.-F. Chen, L.-T. Jin, B.-R. Cheng, F. Hu, B. Xiong, Fourier transform infrared spectroscopy for the distinction of MCF-7 cells treated with different concentrations of 5-fluorouracil, J. Transl. Med. 13(1) (2015) 1-8.

[31] Z. Sabouri, A. Akbari, H.A. Hosseini, A. Hashemzadeh, M. Darroudi, Bio-based synthesized NiO nanoparticles and evaluation of their cellular toxicity and wastewater treatment effects, J. Mol. Struct. 1191 (2019) 101-109.

[32] M. Alikhani, M. Hakimi, K. Moeini, V. Eigner, M. Dusek, Synthesis, characterization and thermal studies of a nanosized 1D l-arginine/copper(II) coordination polymer by sonochemical method: a new precursor for preparation of copper (II) oxide nanoparticles, J. Inorg. Organomet. Polym. 30(8) (2020) 2907-2915.

[33] I. Gholamali, S.N. Hosseini, E. Alipour, M. Yadollahi, Preparation and characterization of oxidized starch/CuO nanocomposite hydrogels applicable in a drug delivery system, Starch-Stärke 71(3-4) (2019) 1800118.

[34] M. Arfan, D.N. Siddiqui, T. Shahid, Z. Iqbal, Y. Majeed, I. Akram, R. Bagheri, Z. Song, A. Zeb, Tailoring of nanostructures: Al doped CuO synthesized by composite-hydroxide-mediated approach, Results Phys. 13 (2019) 102187.

[35] M. Hakimi, M. Alikhani, Characterization of α-Fe_2O_3 nanoparticles prepared from a new [Fe(Ofloxacin)$_2$Cl$_2$] precursor: a heterogeneous photocatalyst for removal of methylene blue and ciprofloxacin in water, J. Inorg. Organomet. Polym. Mater. 30(2) (2020) 504-512.

[36] K. Lingaraju, H.R. Naika, K. Manjunath, G. Nagaraju, D. Suresh, H. Nagabhushana, Rauvolfia serpentina-mediated green synthesis of CuO nanoparticles and its multidisciplinary studies, Acta Metall. Sin. (Engl. Lett.). 28(9) (2015) 1134-1140.

[37] D.O.B. Apriandanu, Y. Yulizar, Tinospora crispa leaves extract for the simple preparation method of CuO nanoparticles and its characterization, Nano-Struct. Nano-Objects. 20 (2019) 100401.

[38] M. Alagiri, S. Ponnusamy, C. Muthamizhchelvan, Synthesis and characterization of NiO nanoparticles by sol–gel method, J. Mater. Sci.: Mater. Electron. 23(3) (2012) 728-732.

[39] S. Honary, F. Zahir, Effect of zeta potential on the properties of nano-drug delivery systems-a review (Part 2), Trop. J. Pharm. Res. 12(2) (2013) 265-273.

[40] W.W. Andualem, F.K. Sabir, E.T. Mohammed, H.H. Belay, B.A. Gonfa, Synthesis of Copper Oxide Nanoparticles Using Plant Leaf Extract of Catha edulis and Its Antibacterial Activity, J. Nanotechnol. 2020 (2020) 2932434.

[41] A. Iqbal, A.u. Haq, G.A. Cerrón-Calle, S.A.R. Naqvi, P. Westerhoff, S. Garcia-Segura, Green synthesis of flower-shaped copper oxide and nickel oxide nanoparticles via capparis decidua leaf extract for synergic adsorption-photocatalytic degradation of pesticides, Catalysts 11(7) (2021) 806.

[42] R. Khan, M.A. Inam, D.R. Park, S. Khan, M. Akram, I.T. Yeom, The removal of CuO nanoparticles from water by conventional treatment C/F/S: the effect of pH and natural organic matter, Mol. 24(5) (2019) 914.

[43] M. Zakeri, J. Fassihi, Production of Nanogold Particles by Biomass (Wheat) and Investigation on Effective Parameters, Nashrieh Shimi va Mohandesi Shimi Iran 30(2) (2011) 35-41.

[44] S. Tummala, K. Gowthamarajan, M. Satish Kumar, A. Wadhwani, Oxaliplatin immuno hybrid nanoparticles for active targeting: an approach for enhanced apoptotic activity and drug delivery to colorectal tumors, Drug Deliv. 23(5) (2016) 1773-1787.

[45] M. Shafagh, F. Rahmani, N. Delirezh, CuO nanoparticles induce cytotoxicity and apoptosis in human K562 cancer cell line via mitochondrial pathway, through reactive oxygen species and P53, Iran. J. Basic Med. Sci. 18(10) (2015) 993-1000.

DOI: 10.30473/IJAC.2026.78642.1351

Iranian Journal of Analytical Chemistry 12 (2026) 94-104

نانوذرات اکسید مس سنتز شده به روش سبز به عنوان نانوحامل‌های بالقوه برای عامل ضد سرطان ۵-فلورواوراسیل

عفت اسماعیلی شهری
بخش شیمی، دانشگاه پیام نور، تهران، ایران.
* E-mail: ef.esmaili@yahoo.com

تاریخ دریافت: ۱۱ مرداد ۱۴۰۴ **تاریخ پذیرش:** ۲۲ شهریور ۱۴۰۴

چکیده

نانوذرات اکسید مس با روش سل-ژل سبز با استفاده از عصاره آبی برگ گیاه علف مورچه و نیترات مس (II) به عنوان پیش‌ساز مس تهیه شدند. نانوذرات حاصل متعاقباً به عنوان حامل برای داروی ضد سرطان ۵-فلورواوراسیل استفاده شدند .مشخصه‌یابی فیزیکوشیمیایی با استفاده از طیف‌سنجی مادون قرمز تبدیل فوریه (FTIR)، طیف‌سنجی فرابنفش-مرئی (UV-Vis)، پراش پرتو ایکس (XRD)، میکروسکوپ الکترونی روبشی گسیل میدانی همراه با طیف‌سنجی پراش انرژی پرتو ایکس (FESEM/EDX)، پراکندگی نور دینامیکی (DLS)، اندازه‌گیری پتانسیل زتا و آنالیز حرارتی-وزن‌سنجی/ تفاضلی (TGA/DTA) انجام شد. راندمان بارگذاری دارو با کروماتوگرافی مایع با کارایی بالا (HPLC) تعیین شد و تأثیر pH محیط واکنش، زمان تماس و غلظت نانوذرات بر عملکرد بارگذاری به طور سیستماتیک برای شناسایی شرایط بهینه بررسی شد. نانوذرات اکسید مس سنتز شده کروی، بسیار خالص و دارای ساختار کریستالی مکعبی با اندازه متوسط ذرات تقریباً ۳۹ نانومتر و پتانسیل زتا ۱۵٫۶- میلی‌ولت بودند .تحت شرایط بارگذاری بهینه (pH 5.50، زمان تماس ۵ ساعت، ۰/۰۱۵ گرم نانوذرات اکسید مس)، تقریباً ۴۰٪ از داروی ۵-فلورواوراسیل روی سطح نانوذرات بارگزاری شد. سنجش سمیت سلولی MTT، مرگ سلولی وابسته به غلظت را در سلول‌های کارسینوم هپاتوسلولار Huh-7 با IC50 تقریباً ۲۵۰ میلی‌گرم در لیتر نشان داد، نتیجه‌ای که با مشخصات زیست‌سازگاری قابل قبول است.

کلید واژه‌ها

روش سبز، علف مورچه، نانوذرات اکسید مس، بارگذاری دارو، ۵-فلورواوراسیل.

DOI: 10.30473/IJAC.2026.78642.1351